Supplementary Material for the Article Entitled: Analysis of Radiation Pressure and Aerodynamic Forces Acting on Powder Grains in PBAM.

Sina Haeri[a,*], Soroush Haeri[b], Jack Hanson[a], Saeid Lotfian[c]

[a] *James Weir Fluid Laboratory, Department of Mechanical and Aerospace Engineering, University of Strathclyde, 75 Montrose St, Glasgow, UK, G1 1XQ.*
[b] *Simon Fraser University, Vancouver, British Columbia, Canada*
[c] *Department Of Naval Architecture, Ocean Marine Engineering, University of Strathclyde, Glasgow, UK, G4 0LZ.*

Abstract

The supplementary material for the paper entitled "Analysis of Radiation Pressure and Aerodynamic Forces Acting on Powder Grains in Powder-Based Additive Manufacturing" is provided here. Various correlations used for the calculation of the drag and lift forces, procedures for the estimation of velocity profiles, the generalised Lorenz-Mie theory used for the calculation of the radiation pressure and optical properties of the Inconel powder are detailed in this document.

Keywords:

1. Introduction

The correlations used here for the calculation of aerodynamic forces are chosen based on the predicted values for Re, Kn and Ma at process conditions. To model the full process, these correlations can be used in conjunction with a particle-based modeling framework such as the Discrete Element Method (DEM) [1, 2] and unresolved coupling techniques [3–6] to predict the collective behaviour of a bed of powder or to guide the fully resolved simulations [7–11] for applying the appropriate boundary conditions. The radiation pressure is calculated using the generalised Lorenz-Mie theory [12–15] which is valid for any particle diameter to wavelength ratio. Further details are provided in the following sections.

*Corresponding author
Email address: sina.haeri@strath.ac.uk (Sina Haeri)

2. Material

For the representative calculations in this paper we assume Inconel 718 (IN718) powder. The density and diameter of an IN718 grain are set to $\rho_p = 8180$ kg/m^3 and $D_p = D_{50} = 30$ μm, respectively [16]. For simplicity, the complex refractive index of nickel at 1.14 eV ($\lambda \approx 1.09$ μm), hence $n_r = 2.65 + 5.93$i, is considered in this paper [17].

3. Calculation of Aerodynamic Forces

In order to calculate the aerodynamic forces, a Reynolds number is defined as $\mathrm{Re} = \rho_f U D_p/\mu_f$, where, ρ_f, U, and μ_f are the density, a characteristic velocity, defined as $|U_f - U_p|$, and the viscosity of the fluid, respectively.

Argon gas is assumed as the inert atmosphere at 1.0 bar and its density ρ_f is calculated using the ideal gas law by assuming a linear variation of the temperature with respect to the laser power. As suggested in [18], laser intensities in the range of 50 to 200 W

with the corresponding temperatures in the range of 5×10^3 to 7×10^3 are considered in the manuscript. In Figure 2a of the manuscript, 6 different laser powers between 50 to 100 W and 5 powers between 120 to 200 W are selected in increments of 10 and 20, respectively. The corresponding temperatures between 5×10^3 to 7×10^3 K are then calculated using linear interpolation.

The viscosity at very high-temperatures is calculated by adding the contributions of the dilute gas viscosity $\mu_0(T)$ and the residual viscosity $\mu_r(\tau, \sigma)$, where T denotes the temperature, $\tau = T_c/T$, and $\sigma = P/P_c$ with T_c and P_c being the critical temperature and pressure. The correlations for μ_0 and μ_r depend on Lennard-Jones parameters for argon [19].

By assuming that the particles are small compared to the curvature of the flow streamlines, the Faxén terms may be ignored [20]. The maximum calculated Re ≈ 12 and hence the following Schiller–Naumann equation is used for the calculation of drag force (valid for Re < 800):

$$\begin{aligned} F_D &= \frac{\rho_f C_D A}{2}(U_f - U_p)^2, \text{ with} \\ C_D &= \frac{24 f_1(\mathrm{Kn})}{(1+\mathrm{Ma}^4)\mathrm{Re}}(1 + 0.15\mathrm{Re}^{0.681}) + \\ &\quad \frac{\mathrm{Ma}^4 f_2(\mathrm{Re}, \mathrm{Ma})}{1+\mathrm{Ma}^4}, \end{aligned} \tag{1}$$

where A, Kn and Ma denote the area of the corss-section, Kundsen and Mach numbers respectively [21]. Furthermore, the f_1 and f_2 functions are used respectively to correct for the effects of rarefaction and compressibility. The maximum Mach number is $\mathrm{Ma} = U_f/\sqrt{\gamma RT} = 0.77$ and the Knudsen number $\mathrm{Kn} = \sqrt{\pi\gamma/2}\mathrm{Ma}/\mathrm{Re} = 0.11$, which suggests that the rarefaction (via f_1) and compressibility (via f_2 and the Ma^4 factor) effects should be considered. The correlations for f_1 an f_2 are given by [22]:

$$\begin{cases} f_1 = \left\{1 + \left[2.514 + 0.8\exp(-0.55\mathrm{Kn}^{-1})\right]\mathrm{Kn}\right\}^{-1} \\ f_2 = \left[1 + (\frac{f}{1.63} - 1)\sqrt{\frac{\mathrm{Re}}{45}}\right]^{-1} f, \end{cases} \tag{2}$$

where, f is given by

$$f = \frac{(1+2s^2)\exp(-s^2)}{s^3\sqrt{\pi}} + \frac{(4s^4+4s^2-1)\mathrm{erf}(s)}{2s^4}. \tag{3}$$

In Eq. (3), $s = \mathrm{Ma}\sqrt{\frac{\gamma}{2}}$ and erf is the error function.

The Saffman and Magnus lift forces also act on the particles during the process. The Magnus force is not considered since the particles are micron-size and initially assumed to be at rest resulting in a spin ratio $\Omega_p = 0.5 D_p \omega_p / |U_f - U_p| \approx 0$, where ω_p is the particle angular velocity [20]. However, Saffman lift [20], is considered by assuming that the grains lie on the surface of the bed and downward lift is assumed positive (z-direction), and thus, the general equation for Saffman lift is simplified as:

$$F_S = 1.61 C_S D_p^2 (\mu_f \rho_f \omega_f)^{0.5}(U_f - U_p), \tag{4}$$

where $\omega_f = \frac{dU_f}{dy}$. Furthermore, C_S is calculated according to [23]:

$$C_S = (1 - 0.3314\beta^{0.5})\exp(-\frac{\mathrm{Re}}{10}) + 0.3314\beta^{0.5}, \tag{5}$$

where, $\beta = \frac{D_p}{2|U_f - U_p|}|\omega_f|$. The velocity gradient, $\frac{dU_f}{dy}$ is calculated using a first order forward difference based on the radial velocity data available at different heights from the bed.

Even though the compressibility and rarefaction could in fact affect F_S, in the absence of reliable correlations, these effects may be ignored. The maximum error in the calculation of F_D before applying the corrections (f_1, f_2 and Ma^4 factor) is %Err = 27 and therefore, at worst, errors of similar order are expected in the estimated values of F_S.

4. Calculation of grain weight and inertia

The particle weight is calculated as $W_p = \pi/6 D_p^3 \rho_p g$ and the buoyancy effects are ignored. Moreover, the Stokes number is defined as $\mathrm{St} = \rho_p U D_p^2 f_1(\mathrm{Kn})/(18\mu_f w_0)$, where the laser waist diameter w_0 is used as the characteristic length scale.

5. Radiation Pressure

For various PBAM processes the grain size is at best one order of magnitude larger than the laser wavelength λ. Therefore, in order to achieve the most reliable results generalised Lorenz-Mie theory is employed here. The radiation pressure on a particle, which is arbitrarily positioned in a Gaussian beam in longitudinal (normal to the bed) and transverse (tangential to the bed) directions, are respectively given by [15]:

$$\begin{aligned} F_{L,z} = \frac{2I}{c}(\frac{\lambda}{\pi r_0})^2 \sum_{n=1}^{\infty}\sum_{p=-n}^{n}\Big[\frac{1}{(n+1)^2}\frac{(n+1+|p|)!}{(n-|p|)!} \\ \times \Re\big[(a_n + a_{n+1}^* - 2a_n a_{n+1}^*)g_{n,TM}^p g_{n+1,TM}^{p*} \\ + (b_n + b_{n+1}^* - 2b_n b_{n+1}^*)g_{n,TE}^p g_{n+1,TE}^{p*}\big] \\ + p\frac{2n+1}{[n(n+1)]^2}\frac{(n+|p|)!}{(n-|p|)!} \\ \times \Re\big[\mathrm{i}(2a_n b_n^* - a_n - b_n^*)g_{n,TM}^p g_{n,TE}^{p*}\big]\Big], \end{aligned} \tag{6}$$

and

$$\begin{aligned} \mathcal{F} = \frac{2I}{c}(\frac{\lambda}{\pi r_0})^2 \sum_{p=1}^{\infty}\sum_{n=p}^{\infty}\sum_{\substack{m=p-1 \\ m\neq 0}}^{\infty}\frac{(n+p)!}{(n-p)!} \\ \times \Big[(S_{m,n}^{p-1} + S_{n,m}^{-p} - 2U_{m,n}^{p-1} - 2U_{n,m}^{-p}) \\ \times (\frac{\delta_{m,n+1}}{m^2} - \frac{\delta_{n,m+1}}{n^2}) + \frac{2n+1}{[n(n+1)]^2} \\ \times \delta_{m,n}(T_{m,n}^{p-1} - T_{n,m}^{-p} - 2V_{m,n}^{p-1} + 2V_{n,m}^{-p})\Big], \end{aligned} \tag{7}$$

where c is the speed of light in vacuum, I is the total laser power, and $r_0 = 2w_0$ is the waist radius (see Figure 1). The coefficients a_n and b_n are the classical scattering coefficients of generalised Lorenz-Mie theory [12, 13] given by:

$$a_n = \frac{\mu_p\psi_n(\alpha)\psi_n'(\beta) - \mu_g n_r\psi_n'(\alpha)\psi_n(\beta)}{\mu_p\xi_n(\alpha)\psi_n'(\beta) - \mu_g n_r\xi_n'(\alpha)\psi_n(\beta)} \tag{8}$$

$$b_n = \frac{\mu_g n_r\psi_n(\alpha)\psi_n'(\beta) - \mu_p\psi_n'(\alpha)\psi_n(\beta)}{\mu_g n_r\xi_n(\alpha)\psi_n'(\beta) - \mu_p\xi_n'(\alpha)\psi_n(\beta)}. \tag{9}$$

where, $\alpha = \frac{\pi D_p}{\lambda}$, $\beta = n_r\alpha$, $\phi_n(z)$ and $\xi_n(z)$ are the Riccati–Bessel functions, which are defined based on the spherical Bessel function [24], and μ_p and μ are the permeabilities of the particle and scattering medium. In Eqs. (6) and (7), $g_{n,TM(TE)}^p$ are the beam shape coefficients, which may be accurately and efficiently calculated using a set of twenty finite series [14]. The terms $T_{n,m}^p$, $S_{n,m}^p$, $U_{n,m}^p$, and $V_{n,m}^p$ are functions of $g_{n,TM(TE)}^p$, a_n, b_n, and their complex conjugates (represented by a star superscript in Eqs. (6) and (7)) and are provided in [15]. Furthermore, the forces $F_{L,x}$ and $F_{L,y}$ are given by $\Re(\mathcal{F})$ and $\Im(\mathcal{F})$, respectively.

6. Further particulars

Two different regions are considered in this paper, the vapour jet region and the radial flow region. It is assumed that the flow velocity U_f is normal to the bed's surface (opposite to the laser longitudinal direction) in the vapour jet region and tangential to the surface in the radial flow region. Without loss of generality, it is assumed that the laser is circularly polarized. Therefore, a 2D coordinate system may be used and it may be assumed that the radial drag is in x-direction, see Figure 1. In the absence of reliable experimental data, the data presented by Bidare et al. [18] is used to estimate the fluid velocities. The velocity profiles reported in Bidare et al. [18] are merely the results of the finite element analysis.

References

[1] S. Haeri, Y. Wang, O. Ghita, J. Sun, Powder Technology 306 (2017) 45–54.

[2] S. Haeri, Powder Technology 321 (2017) 94–104.

[3] S. Haeri, J. Shrimpton, Progress in Energy and Combustion Science 37 (2011) 716–740. doi:10.1016/j.pecs.2011.03.002.

[4] S. Haeri, J. S. Shrimpton, International Journal of Multiphase Flow 40 (2012) 38–55.

[5] J. S. Shrimpton, S. Haeri, S. Scott, Statistical Treatment of Turbulent Polydisperse Particle Systems, Green Energy and Technology, Springer, 2014.

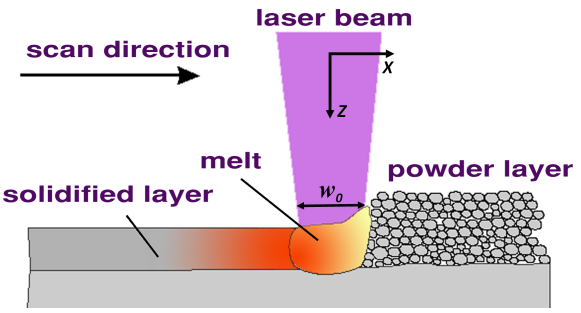

Figure 1: A schematic presentation of the SLM process. A thin layer of powder is spread on a build plate and a thermal energy source is used to selectively fuse the regions of powder bed at desired locations based on a CAD model. After completion of a layer, a repetition of the fabrication process will be accomplished by applying a new layer of powder until a 3D component is fabricated.

[6] S. Haeri, L. Benedetti, O. Ghita, Powder Technology 363 (2020) 245–255.

[7] S. Haeri, J. S. Shrimpton, Journal of Computational Physics 237 (2013) 21–45.

[8] S. Haeri, J. Shrimpton, International Journal of Heat and Mass Transfer 59 (2013) 219–229. doi:10.1016/j.ijheatmasstransfer.2012.12.012.

[9] S. Haeri, J. S. Shrimpton, International Journal of Heat and Fluid Flow 50 (2014) 1–15.

[10] Y. Zhang, G. Pan, Y. Zhang, S. Haeri, Computer Methods in Applied Mechanics and Engineering 352 (2019) 675–690.

[11] Y. Zhang, G. Pan, Y. Zhang, S. Haeri, Computer Physics Communications 248 (2020) 106980.

[12] H. C. van de Hulst, Light scattering by small particles, John Wiley and Sons, 1957.

[13] C. F. Bohren, D. R. Huffman, Absorption and Scattering of Light by Small Particles, Wiley-VCH Verlag GmbH, 2004.

[14] G. Gouesbet, G. Grehan, B. Maheu, Journal of optics 19 (1988) 35–47.

[15] K. F. Ren, G. Greha, G. Gouesbet, Optics Communications (1994).

[16] Q. B. Nguyen, M. L. S. Nai, Z. Zhu, C.-N. Sun, J. Wei, W. Zhou, Engineering 3 (2017) 695 – 700.

[17] P. B. Johnson, R. W. Christy, Physical Review B (1974).

[18] P. Bidare, I. Bitharas, R. M. Ward, M. M. Attallah, A. J. Moore, Acta Materialia 142 (2018) 107–120.

[19] E. W. Lemmon, R. T. Jacobsen, International Journal of Thermophysics 25 (2004) 21–69.

[20] C. T. Crowe, J. D. Schwarzkopf, M. Sommerfeld, Y. Tsuji, Multiphase Flows with Droplets and Particles, CRC Press, 2011. Chapter 4.

[21] P. P. Brown, D. F. Lawler, Journal of Environmental Engineering 129 (2003) 222–231.

[22] E. Loth, AIAA 46 (2008) 2219–2228.

[23] R. Mie, International Journal of Multiphase Flow 18 (1992) 145–147.

[24] G. Gouesbet, G. Gréhan, Generalized Lorenz-Mie Theories, second ed., Springer, 2017.